Journal of Nuclear Materials 389 (2009) 341–350

Contents lists available at ScienceDirect

Journal of Nuclear Materials

journal homepage: www.elsevier.com/locate/jnucmat

MgO–pyrochlore composite as an inert matrix fuel: Neutronic and thermal characteristics

A. Imaura [a], N. Touran [b], R.C. Ewing [a,b,*]

[a] Department of Geological Sciences, University of Michigan, Ann Arbor, MI 48109-1005, United States
[b] Nuclear Engineering and Radiological Sciences, University of Michigan, Ann Arbor, MI 48109-1005, United States

ARTICLE INFO

Article history:
Received 5 November 2008
Accepted 8 January 2009

ABSTRACT

Inert matrix fuels are an important component of advanced nuclear fuel cycles, as they provide a means of utilizing plutonium and reducing the inventory of 'minor' actinides. We examine the neutronic and thermal characteristics of MgO–pyrochlore ($A_2B_2O_7$: $La_2Zr_2O_7$, $Nd_2Zr_2O_7$ and $Y_2Sn_2O_7$) composites as inert matrix fuels in boiling water reactors. By incorporating plutonium with resonance nuclides, such as Am, Np and Er, in the A-site of pyrochlore, the k_{inf} *vs.* burn-up curves are shown to be similar to those of UO_2, although the Doppler coefficients are less negative than UO_2. The Pu depletion rates are 88–90% (^{239}Pu) and 54–58% (total Pu) when the inert matrix fuels experience a burn-up equivalent of 45 GWd/tHM UO_2. Because of the high thermal conductivity of MgO, the center-line temperatures of the MgO–pyrochlore composites at 44.0 kW/m are lower than those of UO_2 pellets. After burn-up, the A-site cation composition is 15–35 at.% lower than that of the B-site cations in pyrochlore (e.g., $A_{1.84}B_{2.17}O_{7.00}$) due to the fission of Pu in the A-site and the presence of fission product elements in the A- and B-sites of the pyrochlore structure.

1. Introduction

The management of Pu either generated in advanced nuclear fuel cycles or from the dismantling of nuclear weapons is a global issue that impacts the long-term sustainability of the uranium resources and the proliferation of nuclear weapons. The consumption of Pu in light water reactors (LWRs) is an excellent means of reducing the Pu-inventory, while extracting the maximum energy from the uranium resource. Presently, a Uranium–Plutonium Mixed Oxide Fuel (MOX) is being considered or used in many countries, such as France, Germany, Belgium, Switzerland, Russia, Japan and the United States (for excess weapon Pu). MOX, however, does not provide for the optimal reduction of Pu inventories because it contains ^{238}U; MOX is also a source of Pu. For this reason, inert matrix fuels (IMFs) have recently received considerable attention [1–3]. These fertile-free fuels have a distinctive advantage in that they allow a much greater degree of reduction of the transuranic (TRU) elements than can be achieved by using MOX fuels [4].

However, the IMFs for LWRs must meet strict material performance requirements that include irradiation stability, high thermal conductivity, low neutron capture cross-sections, and, ideally, good resistance to corrosion in hot, aqueous solutions [4]. In the event that the used IMF is utilized for direct disposal in a geologic repository, high corrosion resistance under the conditions of the geologic repository is also desirable [2]. Many materials, such as magnesia (MgO), rock-like oxides (ROX) composed of spinels ($MgAl_2O_4$), zirconia (ZrO_2), pyrochlore ($A_2B_2O_7$), cercer (ceramics embedded in another ceramic), and cermet (ceramics embedded in metal) [4–7] have been proposed as candidate IMFs, as each of these materials meets some or even all of these requirements. Although some of these materials have been irradiated in reactors in test fuel assemblies, they have not been used in reactors. Because the global inventory of Pu grows at a rate of 70–90 metric tons per year, there is presently a keen interest in developing IMFs.

The isometric pyrochlore structure ($A_2^{3+}B_2^{4+}O_7$) has been the subject of considerable research because it is considered a good nuclear waste form for the incorporation of Pu and 'minor' actinides [8]. Actinides, depending on their oxidation state, can be incorporated into either the A- or B-site. The pyrochlore structure shows remarkable flexibility, and over 500 different compositions have been synthesized. The possibility of synthesizing actinide pyrochlores was first discussed by Chakoumakos and Ewing in 1985 [9] and since that time there have been many studies of actinide-bearing pyrochlores [10–12]. Based on the large number of systematic studies [8], it is now evident that pyrochlore structure-types show a wide range of physical, chemical and electronic properties, depending on their composition. As an example, the zirconate pyrochlores show a remarkable resistance to the radiation-induced transformation from the crystalline state to the amorphous state

* Corresponding author. Address: Department of Geological Sciences, University of Michigan, Ann Arbor, MI 48109-1005, United States.
E-mail address: rodewing@umich.edu (R.C. Ewing).

0022-3115/$ - see front matter © 2009 Elsevier B.V. All rights reserved.
doi:10.1016/j.jnucmat.2009.01.241

[13], except for $La_2Zr_2O_7$ [14]. In addition, Lian et al. [15] have shown that although $La_2Zr_2O_7$ can be amorphized, due to alpha-decay damage from incorporated actinides, the irradiation behavior of $La_2Zr_2O_7$ may be improved by the addition of actinides.

The interest in pyrochlore as an inert matrix fuel is rather recent. Lutique et al. [16] have investigated the thermal conductivity of neodymium zirconate pyrochlore ($Nd_2Zr_2O_7$) both theoretically and experimentally. They concluded that the thermal conductivity of $Nd_2Zr_2O_7$ is too low to be used as a single phase IMF. However, they showed that the expected temperature profiles of MgO–$Nd_2Zr_2O_7$ pellets would be lower than the corresponding profiles for UO_2. MgO is an ideal IMF candidate due to its high thermal conductivity. However, this structure cannot incorporate actinides, and its chemical stability is rather low. Yates et al. [5] proposed that a composite fuel of MgO and pyrochlore could be developed that would have both high thermal conductivity and good chemical durability.

The first step in evaluating the potential of an MgO/pyrochlore composite as an IMF is to evaluate the neutronic characteristics of compositions that have been optimized in terms of the pyrochlore composition. Because of the absence of ^{238}U, which accounts for a sizable portion in the UO_2 fuel, the neutronic characteristics of IMF are very different from those of UO_2. Generally speaking, the Doppler coefficient of an IMF is lower and the reactivity swing of an IMF is larger than that of UO_2 due to the absence of fertile ^{238}U, which has the resonance absorption cross-section [2,7]. In order to deal with the former issue, one may consider adding resonance absorbers, such as Er, Th, and ^{238}U, to IMF fuel pellets [2,3,7]. For the latter issue, one may evaluate the addition of minor actinides (MA), such as Np and Am in order to make the falling gradients of the reactivity curve less. In this case, the addition of a combination of Pu + Np and Pu + Np + Am has been proposed in light of proposed reprocessing strategies that provide a mixture of actinide elements [17].

Yates et al. [5] have discussed several possible compositions of MgO–$Nd_2Zr_2O_7$ from the point of view of the k-effective value. They showed that because of the larger thermal absorption cross-section of Nd, as compared with that of Mg, the best ratio of $Nd_2Zr_2O_7$ to MgO was 3:7 in order to provide enough end-of-life (EOL) reactivity for the case of 8 wt% weapons-grade PuO_2 incorporated into the pyrochlore. They also indicated the need for compositional variations to lower the initial neutron multiplication factor. Importantly, however, in this paper, it is shown that the MgO–pyrochlore can maintain the eigenvalue at EOL despite the existence of lanthanides in matrix. Their analysis does not deal with the issues peculiar to IMF, which include the evaluation of the fuel properties *vs.* the longer term requirements for disposal, e.g., resistance to radiation damage and corrosion.

In this paper, we evaluate the feasibility of using the MgO–pyrochlore composite as an IMF in LWRs with special attention to its neutronic properties and thermal conductivity. We also evaluate the after burn-up compositions in light of important waste form properties, such as corrosion resistance.

2. Analysis

In order to examine the feasibility of MgO–pyrochlore composite as an IMF in LWRs, a series of composite compositions of MgO–pyrochlore were considered in terms of neutron calculations, where both MgO and pyrochlore were assumed to be at 95% theoretical density. The resulting composite compositions are considered in terms of their neutronic, thermal and material properties. The 9 × 9B BWR fuel assemblies, which are currently used in Japan, were used as the basis for the calculation. The major characteristics of the 9 × 9B assembly and its horizontal sectional view are shown in Table 1 and Fig. 1, respectively [18]. This UO_2 assembly was used as the reference for comparison to the calculations of the different IMF compositions.

Table 1
Parameters of the 9 × 9B UO_2 fuel assembly.

			UO_2	(U, Gd)O_2
Pellet	^{235}U Enrichment (wt%)	Ave.	3.74	
		Pin	2.4–4.9	3.4
	BP content (wt%)		–	4.0/5.0
	Density (%T.D.)		97	
	Outer diameter (mm)		9.4	
	Height (mm)		10	
Cladding/rod	Material		Zry-2	
	Outer diameter (mm)		11.0	
	Thickness (mm)		0.7	
	Gap length (mm)		0.2	
Water channel	Material		Zry-2	
	Outer length (mm)		38.5	
Channel box	Material		Zry-2	
	Thickness (mm)		2.5	
Distance	Rod (center) to rod (center) (mm)		14.4	
	Assembly (center) to assembly (center) (mm)		151	

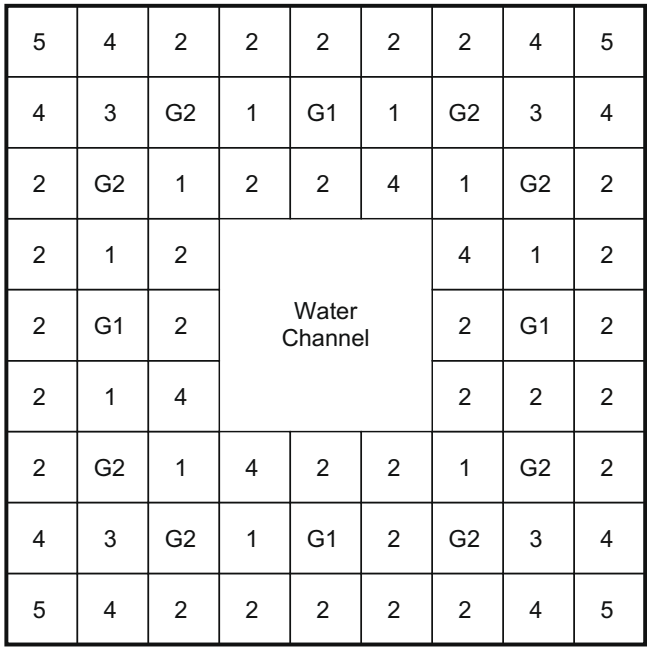

Fig. 1. Rod disposition of UO_2 [18] Rod '3' and 'G2' contain axial enrichment distribution.

In this study, MgO–zirconate pyrochlores, MgO–(Pu, An, Er, La)$_2Zr_2O_7$ and MgO–(Pu, An, Er, Nd)$_2Zr_2O_7$, where An = Am or Np, are discussed first. MgO–(Pu, An, Gd)$_2Zr_2O_7$ are used as 'poison' rods. In addition, another pyrochlore candidate, MgO–(Pu, An, Er, Y)$_2Sn_2O_7$, is finally discussed.

Reactor-grade Pu, with the isotopic composition given below, was used as the fissile component.

^{238}Pu:^{239}Pu:^{240}Pu:^{241}Pu:^{242}Pu:^{241}Am = 2:59:27:8:4:1.

2.1. Neutronic analysis

Two-dimensional 36-group neutron transport and burn-up calculations for IMF and UO_2 assemblies were completed for a single assembly using CPM3 [19]. CPM3 is a nuclear fuel lattice physics burn-up code using arbitrary geometric modeling and determinis-

tic transport theory methods. In this study, the Method of Characteristics was employed for the transport calculations, and the nuclear data were derived from ENDF/B-VI. Since CPM3 does not take into account the ^{238}Pu (n,γ) ^{239}Pu and ^{244}Cm (alpha-decay) ^{240}Pu reactions, these chains were manually added into the nuclear data library of CPM3. In this calculation, the amount of Mg was not considered due to the absence of the necessary material data in CPM3. Taking into account its atomic weight (24.3 u) and small capture cross-section (0.063 barn), however, the influence on the neutron spectrum and eigenvalue is considered to be very limited.

IMF and UO_2 assemblies were assumed to be burned at full power for 1350 days, the total exothermic energy is equivalent to 45 GWd/tHM UO_2, and the void fraction of coolant moderator was set to 40%. The temperatures of IMF and UO_2 pellets were set to 800 K and 900 K, respectively, and held constant in the radial direction. The fuel rod enrichment distribution for IMF was determined as shown in Fig. 2.

In order to make the neutronic performance of the IMF assemblies equivalent to that of the 9×9B UO_2 assemblies, composite compositions were determined by the following constraints:

- The average Pu enrichment was fixed at 0.78 g/cc (Pu_{fis} = 0.52 g/cc) in the horizontal cross-section of the IMF assembly.
- Am or Np were added in appropriate amounts to let the k_{inf} decline versus exposure from the peak to EOL as slight as that of UO_2 in order to make the k_{inf} swing as moderate as that of UO_2.
- Er was added to the whole rods, except for Gd-rods, accompanied with required number of the Gd-rods in order to make the k_{inf} at the beginning of life (BOL) as low as that of UO_2.
- Pyrochlore incorporated with a certain amount of Nd or La was used while keeping the k_{inf} at EOL as high as that of UO_2.

2.2. Thermal analysis

The temperature profiles of the IMF pellets at 44.0 kW/m, which is the maximum linear power density of the 9×9B UO_2 assemblies, were calculated theoretically. The thermal conductivities of MgO and pyrochlore were derived from the literature [16,20,21], assuming that of Pu-doped pyrochlore is the same as $Ln_2Zr_2O_7$ (Ln = La, Nd, Gd). Employing Eq. (1) [22] and Eq. (2) [23], the thermal conductivities of MgO–pyrochlore cercers were calculated by:

$$\lambda_p = \lambda_0(1-p)^{1.7}, \quad (1)$$

where p is the porosity and λ_0 is the thermal conductivity for $p = 0$;

$$\lambda_{eff} = \lambda_D + (1-V_D)(\lambda_M - \lambda_D)(\lambda_{eff}/\lambda_M)^{1/3}, \quad (2)$$

where V_D is the volume fraction of the dispersed phase, and λ_D and λ_M are the thermal conductivities of the dispersed phase and the matrix, respectively.

The temperatures of the pellet centers were obtained from one-dimensional stationary heat equation by using the said thermal conductivities. In this case, the horizontal heat distribution in the pellet was assumed to be constant.

<table>
<tr><td>G2</td><td>3</td><td>G1</td><td>2</td><td>G1</td><td>2</td><td>G1</td><td>3</td><td>G2</td></tr>
<tr><td>3</td><td>1</td><td>1</td><td>1</td><td>1</td><td>1</td><td>1</td><td>1</td><td>3</td></tr>
<tr><td>G1</td><td>1</td><td>1</td><td>G1</td><td>2</td><td>G1</td><td>1</td><td>1</td><td>G1</td></tr>
<tr><td>2</td><td>1</td><td>G1</td><td colspan="3" rowspan="3">Water Channel</td><td>G1</td><td>1</td><td>2</td></tr>
<tr><td>G1</td><td>1</td><td>2</td><td>2</td><td>1</td><td>G1</td></tr>
<tr><td>2</td><td>1</td><td>G1</td><td>G1</td><td>1</td><td>2</td></tr>
<tr><td>G1</td><td>1</td><td>1</td><td>G1</td><td>2</td><td>G1</td><td>1</td><td>1</td><td>G1</td></tr>
<tr><td>3</td><td>1</td><td>1</td><td>1</td><td>1</td><td>1</td><td>1</td><td>1</td><td>3</td></tr>
<tr><td>G2</td><td>3</td><td>G1</td><td>2</td><td>G1</td><td>2</td><td>G1</td><td>3</td><td>G2</td></tr>
</table>

Fig. 2. Rod disposition of IMF (Case 1-3). Pu enrichment decrease from Rod '1' to Rod '3'. Both Pu and Gd enrichments are different between 'G1' and 'G2'.

3. Results and discussion

3.1. Neutronics

By changing the composition of the lanthanides and other additives in pyrochlore, and the number of the Gd-rods, four cases were calculated and considered as shown in Table 2.

Fig. 3 shows the k_{inf} *vs.* burn-up time curves for all cases. Because of the additives, the curves are adjusted to be as moderate as that of UO_2. If the fuels do not contain any additives, such as 'minor' actinides, the k_{inf} curves decrease rapidly since IMFs do not incorporate fertile ^{238}U, but the falling gradients are set to be as slight as that of UO_2 by adding Am or Np. The excessive reactivities at BOL are suppressed by burnable poisons such as Gd and Er. Er can be incorporated into the pyrochlore structure instead of adding additional Er_2O_3 mixed with pyrochlore and MgO.

Table 3 summarizes the composite compositions of the highest Pu enriched rods ('1' in Fig. 2) in the assemblies with the Doppler coefficients and the depletion rate of Pu. The depletion of ^{239}Pu varies from 88.1% to 89.2%, and the depletion of total Pu varies from 54.3% to 58.3% at EOL in Cases 1–4. The difference in the Pu depletion ratio is attributed to the amount of minor actinides added because they function not only as a poison but also as fertile materials for transmutation to ^{239}Pu. Compared with a MOX assembly [18], which is also assumed to reach a burned-up to 45 GWd/tHM, the amount of Pu depletion is at least 2.4 times higher in MgO–pyrochlore cases because IMFs do not supply Pu from fertile ^{238}U during burn-up. The rates of Pu depletion in IMF are also better than those in MOX (63.6% {^{239}Pu}, 33.8% {total-Pu}).

Despite the addition of resonance nuclides such as Am, Np and Er, the Doppler coefficients of MgO–pyrochlore are less negative than those of UO_2. The same effect is also seen in zirconia-based ROX [7] and MgO–ZrO_2 composite [17]. In accordance with precedents [7,17], it is better to use this MgO–pyrochlore IMF assembly mixed with UO_2 assemblies in reactors in order to provide greater compensation for the Doppler coefficient.

In order to assess the adequacy of the loading pattern in an assembly, the Local Peaking Factor (LPF) was checked. LPF, the ratio

Table 2
Case description.

Case no.	Lanthanide	Minor actinide	Number of Gd-rods
Case 1	La	Am	24
Case 2	Nd	Am	24
Case 3	La	Np	24
Case 4	La	Am	22

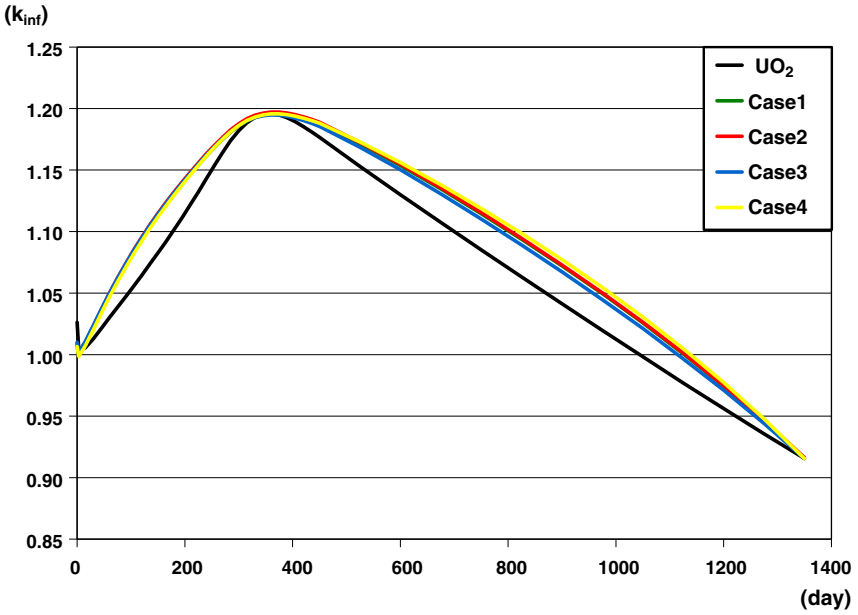

Fig. 3. k_{inf} *vs.* burn-up time curve.

Table 3
Composite compositions of highest Pu enriched rods in assemblies and neutronic characteristics.

Case #	MgO/pyrochlore (vol.%)	Composition of pyrochlore	Doppler[a] (pcm K^{-1})	Pu depletion (%)	
				^{239}Pu	Total
Case 1	47/53	$(Pu_{0.33}\ Am_{0.01}\ Er_{0.01}\ La_{0.65})_2Zr_2O_7$	−0.7	88.6	56.6
Case 2	73/27	$(Pu_{0.62}\ Am_{0.03}\ Er_{0.01}\ Nd_{0.34})_2Zr_2O_7$	−0.7	88.6	56.7
Case 3	76/24	$(Pu_{0.71}\ Np_{0.06}\ Er_{0.01}\ La_{0.22})_2Zr_2O_7$	−0.8	88.1	54.3
Case 4	47/53	$(Pu_{0.33}\ Am_{0.00}\ Er_{0.04}\ La_{0.63})_2Zr_2O_7$	−0.8	89.2	58.3

[a] Doppler coefficient of UO_2 is −1.8.

of maximum pin power to average power in an assembly at a selected height, should be kept as low as possible to comply with the thermal limits. Due to the high radial peaking factor at the end of the 1st cycle and at the beginning of the 2nd cycle [24], special consideration to that period is required as well as to the maximum value of the LPF. As an example, Fig. 4 shows the time dependent curve of the LPF of Case 1. Although the LPF of this period, around 350 days from BOL, is kept low, that of BOL is high because of the well-moderated corner region (Rod 3 in Fig. 2). Since the less negative Doppler coefficient of IMF suggests the need for a UO_2/IMF mixed core, it is necessary to optimize the pin layout in IMF assemblies by taking into account the exchange of thermal neutron flux from neighboring UO_2 assemblies.

In spite of the similarities mentioned above, the MgO/pyrochlore rates and the compositions in the A-site of pyrochlore vary widely in each case, depending on the materials used, such as the type and amounts of lanthanides and minor actinides. Therefore, the differences between cases are discussed in the following section.

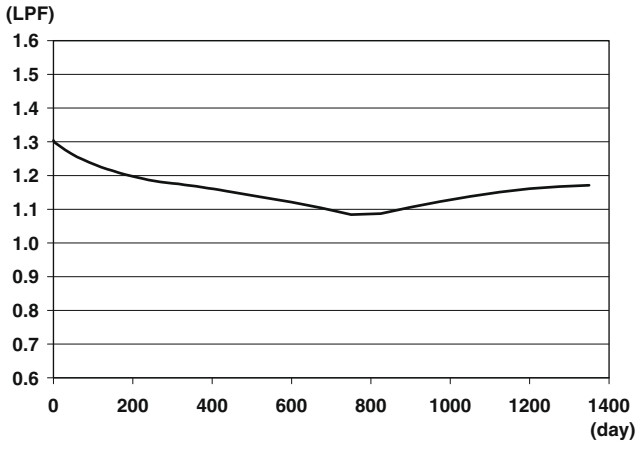

Fig. 4. Local Peaking Factor (LPF) *vs.* burn-up time curve (Case 1).

3.1.1. La vs. Nd

In order to analyze the compositional difference between the use of La *vs.* Nd at the A-site of the pyrochlore, both the MgO–(Pu, Am, Er, La)$_2Zr_2O_7$ (Case 1) and MgO–(Pu, Am, Er, Nd)$_2Zr_2O_7$ (Case 2) were compared. Table 3 demonstrates that both the lanthanide ratio in the A-site of the pyrochlore and the pyrochlore proportion in the MgO–pyrochlore system of La–pyrochlore-based IMF are much larger than those of the Nd–pyrochlore IMF, where the lanthanide ratio in the A-site represents the atomic ratio of La, Nd or Y in the A-site of the pyrochlore at BOL. Because of the smaller absorption cross-section of La (8.97 barn) as compared with Nd (50.5 barn), La–pyrochlore-based IMF is capable of containing about 3.5 times more mass of lanthanide in the IMF system than the Nd–pyrochlore-based IMF. The difference of temperature profiles and composite compositions after burn-up are discussed in the following sections.

3.1.2. Effects of minor actinides (MA)

In order to obtain a reactivity swing that is as moderate as that of UO_2, the addition of MA was examined. At first, to evaluate the usability of each minor actinide, a given amount of MAs was added to all MgO–pyrochlore pellets in the IMF assembles. The obtained values of k_{inf} were compared to values obtained from fuel that did not contain MA. Here, the IMF assemblies are comprised of MgO–(Pu, An, Er, $La)_2Zr_2O_7$ and MgO–(Pu, An, $Gd)_2Zr_2O_7$ pellets, where An = Np(^{237}Np), Am(^{241}Am:^{243}Am = 7:3) or Cm(^{244}Cm). Fig. 5 shows the time dependent effect on k_{inf} when 0.05 g/cc of MA was added to all MgO–pyrochlore pellets in the IMF assembles. The monotonic increase of the Δk after 300 days from BOL provides for the low-gradient reactivity swing, though Cm is less reactive than Am and Np.

From these results, composite compositions that contain Am (Case 1) or Np (Case 3) in the A-site of pyrochlore were determined as shown in Table 3 to make the reactivity curves similar to those of UO_2 (Fig. 3). Since ^{155}Gd shields neutrons from being absorbed by the dominant resonances of ^{237}Np until the Gd burns out and ^{237}Np is less effective at reducing the reactivity swing as shown in Fig. 5, more Np is required in the IMF fuel. The Np-based IMF, however, contains lower amounts of La in the IMF system in order to compensate for the reactivity loss derived from Np at EOL, as shown in Fig. 5. Of course, the amount of La increases linearly with increasing Pu enrichment since the Pu increment compensates for the reactivity loss derived from the additional La. Nevertheless, this increase is unfavorable because the Pu increments result in the deterioration of the Pu depletion rate, when calculated as: (mass of Pu depletion)/(initial mass of Pu).

On the other hand, Am is an ideal material in this system because of its time dependent absorption reactivity throughout the whole burn-up period and its relatively small reactivity loss at EOL. In addition, even though the loading amount is not much (0.037 g/cc), not only the Pu, but also the Am, is transmuted in the reactor; whereas, MOX fuels generally do not contain Am in order to prevent the k_{inf} from decreasing during the burn-up cycle. In this system, the neutron capture is the dominant reaction of ^{241}Am, contrary to fission in fast reactors. Fig. 6 shows the transmutation scheme for ^{241}Am in LWRs presented by Chauvin et al. [25]. Some of ^{241}Am is eventually transmuted to ^{239}Pu and fissioned in the reactor. The rest remains as radioactive heavy metals such as ^{242}Cm at EOL, but their half-lives are shorter than those of ^{237}Np (2.14×10^6 year), the daughter nuclide of ^{241}Am. Therefore, the addition of Am to IMF is useful as a method to not only control reactivity swing, but also provides a mechanism for the depletion of Am itself.

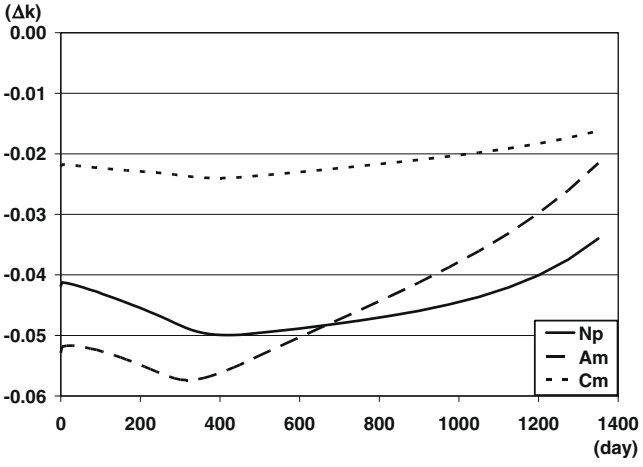

Fig. 5. Effects of addition of minor actinides.

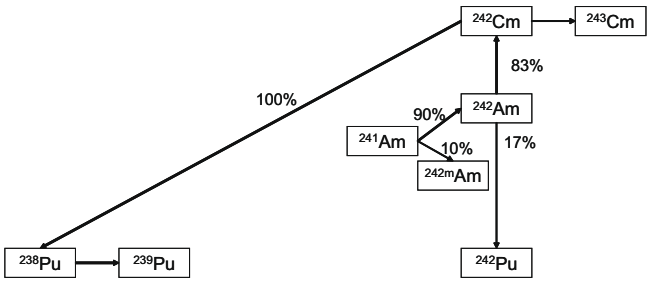

Fig. 6. Transmutation scheme for ^{241}Am in a thermal flux [25].

3.1.3. Effects of Er

In order to suppress the excessive reactivity of the 1st cycle, the end of which is usually located around the peak of the k_{inf} curve, the addition of Er and Gd were considered in this analysis. Er was mixed into all pellets, except for the Gd-pellets. Since Er cannot sufficiently suppress the excessive reactivity, Gd-rods were also employed. In order to evaluate the effects of Er, two cases (Case 1 and Case 4) were calculated based on MgO–(Pu, Am, Er, $La)_2Zr_2O_7$ by changing the number of Gd-rods. To compensate for the lack of Gd-rods at BOL, a larger amount of Er was required in Case 4 than in Case 1. Since the residual reactivity of Er remained after the end of the 1st cycle and linearly reduced its effect depending on the burn-up, Er caused the falling gradient of the k_{inf} from the 2nd cycle to be low with acceptable reactivity loss at EOL in Case 4. As a result, the fuel in Case 4 required less Am than Case 1 did, and provided better Pu depletion, though it does not incinerate Am.

On the other hand, the addition of Er improves the Doppler coefficient. However, the improvement of the Doppler coefficient is limited to between -0.7 pcm K^{-1} in Case 1 and -0.8 pcm K^{-1} in Case 4, the values of which are still worse than those of UO_2. This result confirms that the selection and proportion of Er and MA can be flexibly determined base on the burn-up strategy of the TRU in designs that mix this IMF fuel with UO_2 assemblies in a reactor, as the excess addition of Er cannot bring the Doppler coefficient to values obtained in UO_2.

3.1.4. Correctness of the results from CPM3

The calculation results conducted by CPM3 include uncertainties due to its incomplete nuclear data file. The missing reaction chains, including the neutron capture reaction from ^{238}Pu to ^{239}Pu and the alpha-decay reaction from ^{244}Cm to ^{240}Pu, required revision of CPM3. Since the reaction chains are defined in the nuclear data file of CPM3, these chains were added. Without this modification, CPM3 considers just the capture of ^{238}Pu and alpha-decay of ^{244}Cm, disregarding the production of ^{239}Pu and ^{240}Pu. That is, the depletion of the number density of heavy metal (HM) disagrees with the number of integrated fissions, affecting neutronic parameters such as k_{inf} and the decreasing mass of fuel. Taking into account these reactions, the values of k_{inf} at 45 GWD/tHM are increased by $0.13\%\Delta k/kk'$ (UO_2), $0.44\%\Delta k/kk'$ (MOX), $1.94\%\Delta k/kk'$ (Case 1), respectively. Therefore, this modification is absolutely necessary in order to obtain accurate solutions, not only for the IMF case, but also in the other cases. Though the mass depletion was reduced by 50% by the above revision, the incomplete nuclear data file is still expected to affect the results in the case of calculations for IMF and MOX.

Another deficiency of CPM3 is the absence of ^{243}Cm and ^{245}Cm in the table of nuclides. Since IMF and MOX fuels incorporate TRU from the beginning, a certain amount of HM disappears based on the reactions of the ^{242}Cm (n,γ) ^{243}Cm and ^{244}Cm (n,γ) ^{245}Cm. For example, 0.6% of initially loaded HM is lost based on these reactions in Case 1. Since ^{243}Cm and ^{245}Cm are fissile, this revised code

still underestimates the k_{inf}. On the other hand, the other deficiency is the lack of fission yield data of several heavy metal nuclides, which may offset the deviation of k_{inf}. Because of this, the amount of fission products is less than the one estimated by the integrated fissions. In Case 1, 1.2% of the integrated fissions come from nuclides that do not have fission yield data. Thus, 0.6% of the initially loaded HM fission without producing fission products in the calculation. In addition to above issues, the depletion of poisons and FPs along with their reaction chains contribute at almost 10% of the mass depletion in revised case.

Lastly, the lack of Mg in the nuclear data library in CPM3 also affects the neutronic parameters. The effect from the lack of Mg on k_{inf} was verified in Case 1 by substituting Al or Si in place of Mg, as their atomic masses and cross-sections are relatively similar. The mass densities of the substituting elements in the IMF pellets were fixed to be the same as that of Mg. In both Al and Si cases, the k_{inf} decreased through almost all the burn-up cycle by 0.005 (Δk) on average as compared with the case that does not contain either of them. From these results, the value of k_{inf} would decrease if CPM3 contained the nuclear data of Mg, but the impact should be at most as same as the substitute cases because Mg has a smaller capture cross-section (0.063 barn) than that of Al (0.231 barn) or Si (0.171 barn).

Consequently, the accuracy of the composite composition and the k_{inf} has been greatly improved by the revision of nuclear data file. Indeed, the calculation result on IMF by the revised CPM3 still contains uncertainty, but residual uncertainty on k_{inf} should be small because the effect of the uncertainties offset one another. Furthermore, the discussion based on the results of neutronic calculation should be valid because the trends of the inaccuracies are consistent across all cases.

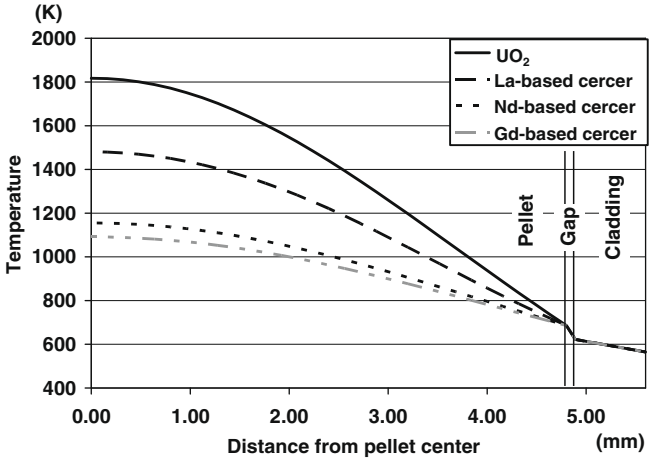

Fig. 7. Temperature profiles of MgO–pyrochlore composite cercer pellets at 44.0 kW/m.

3.2. Thermal properties

Fig. 7 shows the results of the temperature profiles of MgO–$Ln_2Zr_2O_7$ cercer pellets, where Ln = La, Nd and Gd at 44.0 kW/m. Based on the results from the neutronic calculations, especially for Case 1 and 2, the volumetric fraction of the composition of the cercer are as follows; MgO:$La_2Zr_2O_7$ = 47:53, MgO:$Nd_2Zr_2O_7$ = 73:27, MgO:$Gd_2Zr_2O_7$ = 80:20.

Mainly due to the high thermal conductivity of MgO, all of the central temperatures of MgO–pyrochlore are more than 300 K lower than that of UO_2 pellets and have adequate margins for their phase transition and melting temperatures, although this will require experimental confirmation.

3.3. Waste form properties

Since the pyrochlore structure can incorporate lanthanides and actinides into its structure, pyrochlore-based IMF itself is expected to be an acceptable nuclear waste form after it is burned in a reactor. Especially, the zirconate pyrochlores are more suitable to host radioactive elements compared to titanate pyrochlores from the

Table 4
Composite compositions of pyrochlore at 10 years after EOL in Case 1.

Rod #		1	2	3	Gd1	Gd2
Composition[a]		$A_{1.81}B_{2.21}O_{7.00}$	$A_{1.80}B_{2.21}O_{7.00}$	$A_{1.79}B_{2.22}O_{7.00}$	$A_{1.49}B_{2.52}O_{7.00}$	$A_{1.58}B_{2.41}O_{7.00}$
Actinide ratio in the A-site (at.%)		18	16	13	46	20
Isotopic ratio of Pu (%)	^{238}Pu	6	7	8	8	11
	^{239}Pu	17	13	7	11	4
	^{240}Pu	48	46	45	47	33
	^{241}Pu	12	13	13	13	11
	^{242}Pu	16	20	28	22	42

[a] The compositions shown are substoichiometric because we assume that all elements will reside in either the A- or B-sites; however, some elements may not be incorporated into the pyrochlore structure unless there is a change in their oxidation state.

Table 5
Composite compositions of pyrochlore at 10 years after EOL in Case 2.

Rod #		1	2	3	Gd1	Gd2
Composition[a]		$A_{1.63}B_{2.39}O_{7.00}$	$A_{1.61}B_{2.41}O_{7.00}$	$A_{1.58}B_{2.44}O_{7.00}$	$A_{1.49}B_{2.53}O_{7.00}$	$A_{1.58}B_{2.41}O_{7.00}$
Actinide ratio in the A-site (at.%)		39	34	29	45	20
Isotopic ratio ofPu (%)	^{238}Pu	6	7	8	7	11
	^{239}Pu	17	13	7	11	4
	^{240}Pu	48	46	45	47	33
	^{241}Pu	12	14	13	23	11
	^{242}Pu	16	20	28	22	42

[a] The compositions shown are substoichiometric because we assume that all elements will reside in either the A- or B-sites; however, some elements may not be incorporated into the pyrochlore structure unless there is a change in their oxidation state.

Table 6
Atomic composite composition of pyrochlore at 10 years after EOL in Case 1.

	Rod 1 (53vol.%pyrochlore)		Rod 2 (51vol.%pyrochlore)		Rod 3 (50vol.%pyrochlore)		Rod Gd1 (20vol.%pyrochlore)		Rod Gd2 (20vol.%pyrochlore)			
	10y after EOL	(BOL)	10y after EOL	(BOL)	10y after EOL	(BOL)	10y after EOL	(BOL)	10y after EOL	(BOL)		
O	100.00%	(100.00%)	100.00%	(100.00%)	100.00%	(100.00%)	100.00%	(100.00%)	100.00%	(100.00%)	O	
Se	0.02%		0.02%		0.02%		0.04%		0.03%		Se	
Br	0.01%		0.01%		0.01%		0.02%		0.01%		Br	
Kr	0.07%		0.07%		0.08%		0.18%		0.14%		Kr	
Rb	0.07%		0.07%		0.07%		0.17%		0.13%		Rb	
Sr	0.13%		0.13%		0.14%		0.33%		0.26%		Sr	
Y	0.08%		0.08%		0.08%		0.19%		0.15%		Y	A-site
Zr	29.44%	(28.57%)	29.45%	(28.57%)	29.50%	(28.57%)	30.78%	(28.57%)	30.29%	(28.57%)	Zr	B-site
Mo	1.07%		1.09%		1.15%		2.74%		2.14%		Mo	B-site
Tc	0.26%		0.26%		0.27%		0.66%		0.50%		Tc	
Ru	0.97%		0.99%		1.06%		2.49%		2.01%		Ru	B-site
Rh	0.26%		0.25%		0.24%		0.62%		0.39%		Rh	
Pd	0.96%		1.00%		1.09%		2.52%		2.14%		Pd	
Ag	0.06%		0.06%		0.07%		0.16%		0.12%		Ag	
Cd	0.08%		0.09%		0.10%		0.21%		0.20%		Cd	
Sn	0.02%		0.02%		0.02%		0.05%		0.04%		Sn	B-site
Sb	0.00%		0.00%		0.00%		0.01%		0.01%		Sb	
Te	0.14%		0.14%		0.15%		0.36%		0.28%		Te	
I	0.08%		0.08%		0.08%		0.19%		0.14%		I	
Xe	1.36%		1.40%		1.52%		3.54%		2.89%		Xe	
Cs	0.72%		0.71%		0.72%		1.78%		1.29%		Cs	
Ba	0.44%		0.46%		0.49%		1.15%		0.94%		Ba	
La	18.57%	(18.64%)	19.12%	(19.23%)	19.47%	(19.66%)	0.73%		0.58%		La	A-site
Ce	0.86%		0.92%		1.05%		1.31%		1.05%		Ce	A-site
Pr	0.25%		0.25%		0.27%		0.63%		0.49%		Pr	A-site
Nd	0.83%		0.85%		0.90%		2.13%		1.71%		Nd	A-site
Sm	0.20%		0.20%		0.21%		0.50%		0.38%		Sm	A-site
Eu	0.04%		0.05%		0.05%		0.11%		0.09%		Eu	A-site
Gd	0.06%		0.06%		0.07%		5.98%	(5.97%)	13.61%	(13.82%)	Gd	A-site
Er	0.15%	(0.16%)	0.16%	(0.16%)	0.16%	(0.17%)	0.00%		0.00%		Er	A-site
U	0.03%		0.03%		0.02%		0.06%		0.04%		U	A-site
Pu	4.01%	(9.37%)	3.34%	(8.75%)	2.66%	(8.32%)	8.00%	(21.57%)	3.39%	(13.74%)	Pu	A-site
Am	0.61%	(0.40%)	0.57%	(0.42%)	0.48%	(0.43%)	1.34%	(1.03%)	0.73%	(1.01%)	Am	A-site
Cm	0.11%		0.12%		0.13%		0.30%		0.31%		Cm	A-site

point of view of radiation damage stability and leaching behavior [26]. However, the composition of the pyrochlore after burn-up is rather important because this can affect its chemical durability and response to radiation damage during geologic storage.

3.3.1. Composition of waste form after burn-up

Tables 4 and 5 show the summaries of the composite compositions of pyrochlore at 10 years after EOL for Case 1 and Case 2, respectively. The atomic compositions are also shown in Tables 6 and 7, as compared with that at BOL, where the highest burned-up pins are given by their pin number. The atomic compositions are normalized to the ideal oxygen composition of seven per formula unit in pyrochlore. In addition to the initially loaded elements, some of the reactor-derived materials are assumed to be distributed both in the A- and B-sites, as shown in Tables 6 and 7, where Y, lanthanides and actinides are to be incorporated in the A-site, and Zr, Mo, Ru and Sn are at the B-site. An actinide ratio in the A-site represents the atomic ratio of the actinide in the A-site of pyrochlore at 10 years after EOL.

Because of Pu fission and its fission yield, the composition of A-site becomes lower than that of B-site, both in Case 1 (MgO–La-based pyrochlore) and 2 (MgO–Nd-based pyrochlore) as shown in Tables 4 and 5; however, the composition of Case 1 (ex. $A_{1.81}B_{2.21}O_{7.00}$) is more similar to the ideal pyrochlore ($A_2B_2O_7$) than that of Case 2 (ex. $A_{1.63}B_{2.39}O_{7.00}$). Based on the phase diagrams of ZrO_2–$LaO_{1.5}$ and ZrO_2–$NdO_{1.5}$ [27], each of the discharged fuels may contain not only pyrochlore phase but also monoclinic phase depending on the compositional deviation from ideal pyrochlore. From these facts, Case 1 is better than Case 2 in light of its chemical durability. This difference arises from the difference of the lanthanide ratio in the A-site of pyrochlore at BOL. Although La or Nd and Pu occupy a large portion of the A-site of pyrochlore, the quantitative alternation of La or Nd from BOL to EOL is slight; whereas, the depletion of Pu is large. Therefore, Case 1, the lanthanide ratio of which is higher than Case 2, is more similar to ideal pyrochlore stoichiometry than Case 2.

In addition, the actinide ratio in the A-site in Case 1 is smaller than in Case 2 at 10 years after EOL simply because the pyrochlore incorporated a lower ratio of Pu in the A-site of pyrochlore in Case 1 than in Case 2 from the beginning as shown in Table 3. In other words, the lanthanide ratio in the A-site of pyrochlore at the BOL controls the actinide ratio in the A-site of pyrochlore after EOL. Since the higher actinide ratio in pyrochlore provides a higher alpha dose per unit volume, the lower actinide ratio is generally preferable; however, neodymium zirconate pyrochlore (Case 2) does not experience radiation-induced amorphization [26].

3.3.2. Radiation damage

In terms of radiation damage, it is known that zirconate pyrochlores do not experience a radiation-induced transformation from the crystalline to the amorphous state, except for $La_2Zr_2O_7$ [14]. Because of the relatively large ionic radius of La, it can be amorphized, but the critical temperature of this pyrochlore is low (310 K), as shown in Fig. 8. Lian et al. [15] have shown that the irradiation behavior of $La_2Zr_2O_7$ may be improved by the incorporation of actinides due to their generally smaller ionic radii as compared with La. In Case 1, Rod 1 will experience the highest α-dose of all rods, since the Pu density of Rod 1 is at least 1.3 times higher than that of all other rods. Still, the presence of elements whose ionic radii are smaller than La^{3+} (0.1160 nm), such as Pu^{3+} (0.1115 nm), Am^{3+} (0.109 nm) and Er^{3+} (0.1004 nm), as well as other reactor-derived actinides and lanthanides, suggests that there will be an

Table 7
Atomic composite composition of pyrochlore at 10 years after EOL in Case 2.

	Rod 1 (27vol.%pyrochlore) 10y after EOL	(BOL)	Rod 2 (25vol.%pyrochlore) 10y after EOL	(BOL)	Rod 3 (24vol.%pyrochlore) 10y after EOL	(BOL)	Rod Gd1 (20vol.%pyrochlore) 10y after EOL	(BOL)	Rod Gd2 (20vol.%pyrochlore) 10y after EOL	(BOL)		
O	100.00%	(100.00%)	100.00%	(100.00%)	100.00%	(100.00%)	100.00%	(100.00%)	100.00%	(100.00%)	O	
Se	0.03%		0.03%		0.03%		0.04%		0.03%		Se	
Br	0.01%		0.01%		0.01%		0.02%		0.01%		Br	
Kr	0.14%		0.14%		0.15%		0.18%		0.14%		Kr	
Rb	0.13%		0.13%		0.14%		0.17%		0.13%		Rb	
Sr	0.25%		0.26%		0.28%		0.33%		0.26%		Sr	
Y	0.15%		0.15%		0.16%		0.19%		0.15%		Y	A-site
Zr	30.22%	(28.57%)	30.29%	(28.57%)	30.43%	(28.57%)	30.79%	(28.57%)	30.29%	(28.57%)	Zr	B-site
Mo	2.04%		2.13%		2.31%		2.75%		2.15%		Mo	B-site
Tc	0.50%		0.51%		0.55%		0.66%		0.50%		Tc	
Ru	1.83%		1.94%		2.12%		2.50%		2.01%		Ru	B-site
Rh	0.49%		0.49%		0.49%		0.62%		0.39%		Rh	
Pd	1.82%		1.95%		2.18%		2.53%		2.15%		Pd	
Ag	0.12%		0.12%		0.13%		0.16%		0.12%		Ag	
Cd	0.15%		0.17%		0.19%		0.22%		0.20%		Cd	
Sn	0.04%		0.04%		0.04%		0.05%		0.04%		Sn	B-site
Sb	0.01%		0.01%		0.01%		0.01%		0.01%		Sb	
Te	0.27%		0.28%		0.30%		0.36%		0.28%		Te	
I	0.15%		0.15%		0.16%		0.19%		0.14%		I	
Xe	2.59%		2.75%		3.04%		3.55%		2.90%		Xe	
Cs	1.36%		1.39%		1.44%		1.78%		1.29%		Cs	
Ba	0.84%		0.89%		0.98%		1.15%		0.94%		Ba	
La	0.54%		0.57%		0.61%		0.73%		0.58%		La	A-site
Ce	0.97%		1.02%		1.11%		1.32%		1.05%		Ce	A-site
Pr	0.47%		0.49%		0.53%		0.63%		0.49%		Pr	A-site
Nd	11.28%	(9.74%)	11.96%	(10.35%)	12.57%	(10.81%)	2.14%		1.71%		Nd	A-site
Pm	0.01%		0.00%		0.00%		0.01%		0.00%		Pm	A-site
Sm	0.40%		0.42%		0.44%		0.50%		0.38%		Sm	A-site
Eu	0.09%		0.09%		0.10%		0.11%		0.09%		Eu	A-site
Gd	0.11%		0.13%		0.15%		6.00%	(5.99%)	13.63%	(13.84%)	Gd	A-site
Er	0.29%	(0.30%)	0.31%	(0.32%)	0.32%	(0.33%)	0.00%		0.00%		Er	A-site
U	0.05%		0.05%		0.04%		0.06%		0.04%		U	A-site
Pu	7.60%	(17.80%)	6.51%	(17.13%)	5.30%	(16.62%)	7.98%	(21.61%)	3.37%	(13.77%)	Pu	A-site
Am	1.14%	(0.73%)	1.10%	(0.77%)	0.94%	(0.81%)	1.34%	(0.97%)	0.72%	(0.96%)	Am	A-site
Cm	0.20%		0.23%		0.25%		0.29%		0.31%		Cm	A-site

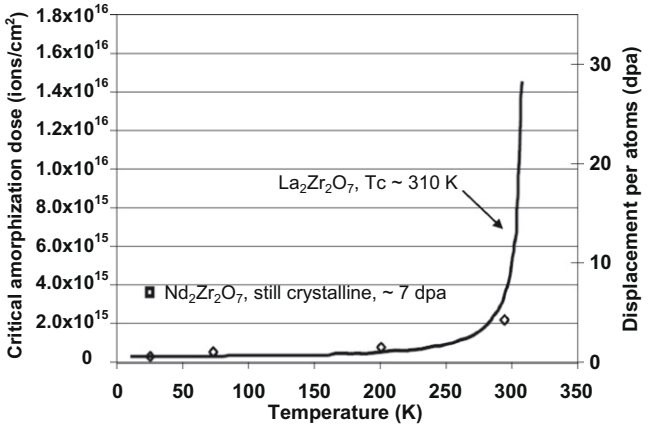

Fig. 8. Temperature dependence of critical amorphization dose of $La_2Zr_2O_7$ irradiated by 1.5-MeV Xe^+ [14].

improvement in the radiation resistance. Although there is now a strong theoretical basis for this prediction [15], this will have to be confirmed experimentally for specific IMF compositions.

3.4. Other pyrochlore candidate compositions

Since the pyrochlore structure can accommodate substantial variations in compositions at the A- and B-sites, other pyrochlores may be good candidates for IMFs: As an example, $Y_2Sn_2O_7$ is among the most radiation resistant of the pyrochlore compositions [28], and it has a small neutron capture cross-section. Lian et al. [28] have shown that there is no evidence of amorphization at room temperature and 25 K (up to doses ~6.82 dpa). From the perspective of the neutronics, $Y_2Sn_2O_7$ has a smaller capture cross-section than $La_2Zr_2O_7$ due to the presence of Y (σ_c; 1.28 barn), although the neutron capture cross-section of Sn (0.626 barn) is greater than that of zirconium (0.194 barn).

Table 8 shows the result of neutronic calculations for MgO–$Y_2Sn_2O_7$ as compared to that of MgO–$La_2Zr_2O_7$ (Case 1) and MgO–$Nd_2Zr_2O_7$ (Case 2). Because of its lower capture cross-section, MgO–$Y_2Sn_2O_7$ requires less Pu loading to maintain the k_{inf} at EOL, while making the lanthanide ratio in the A-site and pyrochlore ratio in MgO–pyrochlore system higher than in Case 1 and 2. Here, the lanthanide ratio in the A-site of pyrochlore stands for the atomic ratio of La, Nd, or Y in the A-site of pyrochlore, as described previously in this paper, even though Y does not belong to lanthanide series. In addition, lower amounts of Pu at initial loading lead to better values than Cases 1 and 2 for the plutonium depletion rate. Furthermore, the actinide ratio in the A-site and the similarity to ideal pyrochlore composition are also better than Cases 1 and 2, owing to the higher lanthanide ratio in the A-site of pyrochlore.

Fig. 9 shows the comparison of composite compositions of these MgO–pyrochlores. The enrichment variation from Rod 1 to Rod 3 of the three materials provides three curves. The upward shift of the curve represents the decrease in the thermal conductivities of MgO–pyrochlores, yet the IMFs would keep them high enough around these rates, owing to MgO's high thermal conductivity. On the other hand, moving to the right represents the increase of the lanthanide content in the A-site, and this results in a closer similarity to an ideal pyrochlore composition, as well as a smaller

Table 8
Calculation results of MgO-$Y_2Sn_2O_7$ compared with MgO-$La_2Zr_2O_7$ (Case 1) and MgO-$Nd_2Zr_2O_7$ (Case 2).

	MgO-$Y_2Sn_2O_7$	MgO-$La_2Zr_2O_7$ (Case 1)	MgO-$Nd_2Zr_2O_7$ (Case 2)
Pu initial loading	0.76g/cc	0.78g/cc	0.78g/cc
Composite composition at BOL[a]	40vol%MgO-60vol%$(Pu_{0.26}Am_{0.01}Er_{0.01}Y_{0.72})_2Sn_2O_7$	47vol%MgO-53vol%$(Pu_{0.33}Am_{0.01}Er_{0.01}La_{0.65})_2Zr_2O_7$	73vol%MgO-27vol%$(Pu_{0.62}Am_{0.03}Er_{0.01}Nd_{0.34})_2Zr_2O_7$
Pu depletion rate at EOL	58.1% (total) 90.2%(^{239}Pu)	56.6% (total) 88.6%(^{239}Pu)	56.7% (total) 88.6%(^{239}Pu)
Actinide ratio in the A-site at 10 years after EOL	10–14 %	13–18 %	29–39 %
Pyrochlore composition at 10 years after EOL[a,b]	$A_{1.84}B_{2.17}O_{7.00}$	$A_{1.81}B_{2.21}O_{7.00}$	$A_{1.63}B_{2.39}O_{7.00}$

[a] The data are about the Rod 1.
[b] The compositions shown are substoichiometric because we assume that all elements will reside in either the A- or B-sites; however, some elements may not be incorporated into the pyrochlore structure unless there is a change in their oxidation state.

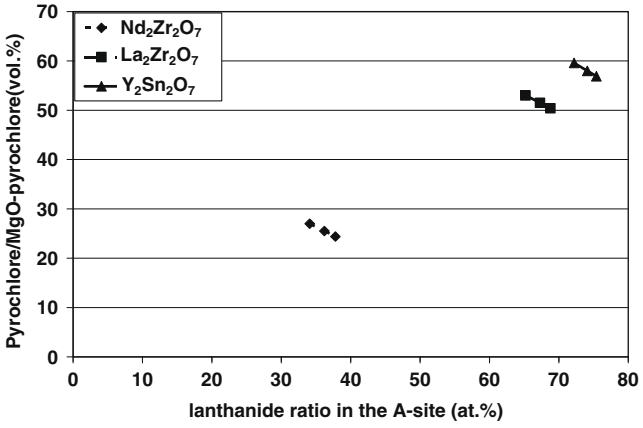

Fig. 9. Composite composition of each rod of MgO–$Y_2Sn_2O_7$, MgO–$La_2Zr_2O_7$ (Case 1), MgO–$Nd_2Zr_2O_7$ (Case2).

actinide ratio after burn-up. Along with the lower capture cross-sections of pyrochlore, the curve moves to the upper right, and $Y_2Sn_2O_7$ showed the best results, followed by $La_2Zr_2O_7$, from not only the neutronic, but also structural point of view.

Because the radiation responses of stannate pyrochlores show a wide variation, depending on the specific cations in the A-site [28], it is unclear whether Pu-bearing $Y_2Sn_2O_7$ will be radiation resistant. Even so, it is meaningful to speculate from the resultant composition. Fig. 10 shows the critical amorphization temperature (T_c)

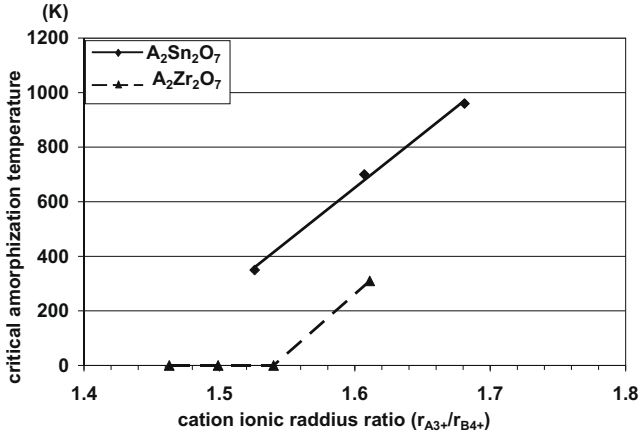

Fig. 10. The critical amorphization temperature (T_c) of stannate pyrochlore irradiated by 1 MeV Kr^{2+} as a function of the cation ionic radius ratio with the data of zirconate pyrochlore composite composition [28].

of stannate pyrochlore irradiated by 1 MeV Kr^{2+} as a function of the cation ionic radius ratio with the data of zirconate pyrochlore presented by Lian et al. [28]. The cation ionic radius ratio of the A- to B-site, r_{A3+}/r_{B4+}, is the parameter most often used to evaluate the radiation response of the pyrochlore structure. The ratio of r_{A3+}/r_{B4+} of these Pu-bearing $Y_2Sn_2O_7$ rods vary from 1.513 (Rod 1) to 1.510 (Rod 3) at BOL and decrease by a factor of a thousand at 10 years after EOL, varying from 1.510 (Rod 1) to 1.505 (Rod 3); whereas, Case 1 varies from 1.604 to 1.608 at 10 years after EOL. Based on the data plotted in Fig. 10, their T_c would be similar to that of MgO–$La_2Zr_2O_7$ (Case 1) and low enough to be annealed at in-reactor temperatures. However, because T_c lies within the range of possible repository temperatures, further experimental studies are required in order to evaluate the radiation response (i.e., the effects of alpha-decay events) during geologic disposal. Nonetheless, the stannate pyrochlore certainly appears to be a promising IMF matrix for actinides.

4. Conclusion

The feasibility of using MgO–pyrochlores ($La_2Zr_2O_7$, $Nd_2Zr_2O_7$ and $Y_2Sn_2O_7$) as IMFs in LWRs has been investigated for the effective transmutation of plutonium. Results from neutronic calculations demonstrated that the k_{inf} *vs.* burn-up curves of MgO–pyrochlore are very similar to that of UO_2, due to the addition of resonance nuclides such as Am, Np and Er into the A-site of pyrochlore with Pu and lanthanides or Y. Here, minor actinides, particularly Am, played the important role of causing the falling gradients of the reactivity curve to be as low as that of UO_2, and the addition of Er suppressed the excessive reactivity at BOL combined with the presence of Gd-rods. Because the residual reactivity of Er caused the falling gradient of the k_{inf} curve to be low, the selection and proportion of Er and MA can be determined based on the burn-up strategy of the TRU. An IMF/UO_2 mixed core is expected to compensate for the less negative Doppler coefficients of the IMF than that of UO_2.

While two zirconate pyrochlore-based IMFs showed similar Pu reduction rates [~89% (^{239}Pu) and ~58% (total Pu)], they had several important differences. Since the relatively large capture cross-section of lanthanides limited the amount of lanthanides that could be included in IMF systems, La–pyrochlore-based IMF incorporated 3.5 times greater mass of lanthanide. Therefore, both the pyrochlore proportion in the MgO–pyrochlore system and the lanthanide ratio in the A-site of pyrochlore of the La–pyrochlore-based IMF were much larger than those of the Nd–pyrochlore IMF. Although the greater pyrochlore proportion in the MgO–pyrochlore system made the pellet temperature profiles attractive, the thermal calculation showed that the pellet center temperatures of MgO–$La_2Zr_2O_7$ at the maximum linear power density were more

than 300 K lower than those of the UO_2 fuel pellets. On the other hand, the lanthanide ratio in the A-site of pyrochlore affected the composite composition of pyrochlore after burn-up, which is important when considering its use as a nuclear waste form for direct geologic disposal. Although the atomic percentage of the A-site cations became lower than that of the B-site in pyrochlore at EOL because of Pu fission and its fission yield, La–pyrochlore-based IMF was more similar to ideal pyrochlore than the Nd–pyrochlore-based IMF.

Since the capture cross-section of $Y_2Sn_2O_7$ is smaller than $La_2Zr_2O_7$, its initial Pu loading was lower, and its lanthanide ratio was higher than zirconate pyrochlore-based IMF. Therefore, the Pu-depletion rates, the similarity to ideal pyrochlore stoichiometry, and the actinide ratio in the A-site, were improved.

For geologic disposal, the radiation resistance was also estimated based on the radius ratio parameter, r_{A3+}/r_{B4+}. $La_2Zr_2O_7$ and $Y_2Sn_2O_7$ are expected to have low critical amorphization temperatures; therefore, the radiation damage will be annealed more quickly and at lower temperatures. However, the radiation response of specific compositions will have to be confirmed experimentally.

Acknowledgements

The senior author thanks the Ministry of Education, Culture, Sports, Science and Technology – Japan and the Japan Patent Office for offering the opportunity to complete this research at the University of Michigan. We acknowledge the gracious help and support of Professor John Lee in the Department of Nuclear Engineering and Radiological Science at the University of Michigan. The authors gratefully acknowledge Ms M. Matice in the English Language Institute at the University of Michigan for her assistance in improving the English.

References

[1] P.G. Boczar, M.J.N. Gagnon, P.S.W. Chan, R.J. Ellis, R.A. Verrall, A.R. Dastur, Can. Nucl. Soc. Bull. 18 (1997) 2.
[2] C. Degueldre, J.M. Paratte, J. Nucl. Mater. 274 (1999) 1.
[3] V.M. Oversby, C.C. McPheeters, C. Degueldre, J.M. Paratte, J. Nucl. Mater. 245 (1997) 17.
[4] W. Carmack, R. Fielding, H.B. Hamilton, P. Medvedev, M. Meyer, J. Nino, S. Philpot, M. Todosow, J. Tulenko, AECL/US INERI – Development of Inert Matrix Fuels for Plutonium and Minor Actinide Management in Power Reactors – Fuel Requirements and Downselect Report, INL/EXT-05-00436, 2005.
[5] S.J. Yates, P. Xu, J. Wang, J.S. Tulenko, J.C. Nino, J. Nucl. Mater. 362 (2007) 336.
[6] IAEA, Viability of Inert Matrix Fuel in Reducing Plutonium Amounts in Reactors, IAEA-TECDOC-1516, 2006.
[7] H. Akie, H. Takano, Y. Anoda, J. Nucl. Mater. 274 (1999) 139.
[8] R.C. Ewing, W.J. Weber, J. Lian, J. Appl. Phys. 95 (11) (2004).
[9] B.C. Chakoumakos, R.C. Ewing, Scientific Basis for Nuclear Waste Management VIII, Mater. Res. Soc. Symp. Proc. 44 (1985) 641.
[10] N.P. Laverov, S.V. Yudintsev, S.V. Stefanovsky, J. Lian, R.C. Ewing, Doklady Russ. Acad. Sci. 376 (5) (2001) 665.
[11] S.V. Yudintsev, S.V. Stefanovsky, O.E. Kiryanova, J. Lian, R.C. Ewing, Phys. Chem. Miner. 1 (2001) 44.
[12] J. Lian, R.C. Ewing, L.M. Wang, S.V. Yudintsev, S.V. Stefanovsky, J. Alloys Compd. 444 & 445 (2007) 429.
[13] S.X. Wang, B.D. Begg, L.M. Wang, R.C. Ewing, W.J. Weber, K.V. Govidan Kutty, J. Mater. Res. 14 (1999) 4470.
[14] J. Lian, X.T. Zu, K.V.G. Kutty, J. Chen, L.M. Wang, R.C. Ewing, Phys. Rev. B 66 (2002) 054108.
[15] J. Lian, L.M. Wang, R.G. Haire, K.B. Helean, R.C. Ewing, Nucl. Instrum. and Meth. Phys. Res. B 218 (2004) 236.
[16] S. Lutique, R.J.M. Konings, V.V. Rondinella, J. Somers, T. Wiss, J. Alloys Compd. 352 (2003) 1.
[17] W.J. Carmack, M. Todosow, M.K. Meyer, K.O. Pasamehmetoglu, J. Nucl. Mater. 352 (2006) 276.
[18] K. Oguchi, Patent Publication JP-2002-372594A.
[19] D.B. Jones, K.E. Watkins, B.D. Paulson, EPRI RP-3418, Electric Power Research.
[20] Y.S. Touloukian, R.W. Powell, C.Y. Ho, P.G. Klemens, Thermophysical Properties of Matter: TPRC Data Series, vol. 2, Plenum, New York, 1970.
[21] G. Suresh, G. Seenivasan, M.V. Krishnaiah, P.S. Murti, J. Nucl. Mater. 249 (1997) 259.
[22] K. Bakker, H. Kwast, E.H.P. Cordfunke, J. Nucl. Mater. 226 (1995) 128.
[23] J.V. Miller, Report NASA-TN-D-3898, 1967.
[24] K. Hida, Y. Hirano, T. Nakajima, Patent Publication JP-2001-228277A.
[25] N. Chauvin, R.J.M. Konings, H. Matzke, J. Nucl. Mater. 274 (1999) 105.
[26] S. Lutique, D. Staicu, R.J.M. Konings, V.V. Rondinella, J. Somers, T. Wiss, J. Nucl. Mater. 319 (2003) 59.
[27] C. Wang, Experimental and Compositional Phase Studies of the ZrO_2-Base Systems for Thermal Barrier Coatings, PhD Thesis, University of Stuttgart, 2006.
[28] J. Lian, K.B. Helean, B.J. Kennedy, L.M. Wang, A. Navrotsky, R.C. Ewing, Phys. Chem. B 110 (5) (2006) 2343.